Nanotechnology in Plant Disease Management: DNA-Directed Silver Nanoparticles on Graphene Oxide as an Antibacterial against *Xanthomonas perforans*

Ismail Ocsoy,[†] Mathews L. Paret,[†] Muserref Arslan Ocsoy,[†] Sanju Kunwar,[†] Tao Chen,[†,‡] Mingxu You,[†,‡] and Weihong Tan[†,‡,*]

[†]Center for Research at the Bio/Nano Interface, Department of Chemistry and Shands Cancer Center, University of Florida, Gainesville, Florida 32611, United States, and Plant Pathology Lab, North Florida Research and Education Center, University of Florida, Quincy, Florida 32351, United States and [‡]Molecular Science and Biomedicine Laboratory, State Key Laboratory of Chemo/Bio-Sensing and Chemometrics, College of Chemistry and Chemical Engineering, College of Biology, Collaborative Innovation Center for Chemistry and Molecular Medicine, Hunan University, Changsha, 410082, China

ABSTRACT Bacterial spot caused by *Xanthomonas perforans* is a major disease of tomatoes, leading to reduction in production by 10−50%. While copper (Cu)-based bactericides have been used for disease management, most of the *X. perforans* strains isolated from tomatoes in Florida and other locations worldwide are Cu-resistant. We have developed DNA-directed silver (Ag) nanoparticles (NPs) grown on graphene oxide (GO). These Ag@dsDNA@GO composites effectively decrease *X. perforans* cell viability in culture and on plants. At the very low concentration of 16 ppm of Ag@dsDNA@GO, composites show excellent antibacterial capability in culture with significant advantages in improved stability, enhanced antibacterial activity, and stronger adsorption properties. Application of Ag@dsDNA@GO at 100 ppm on tomato transplants in a greenhouse experiment significantly reduced the severity of bacterial spot disease compared to untreated plants, giving results similar to those of the current grower standard treatment, with no phytotoxicity.

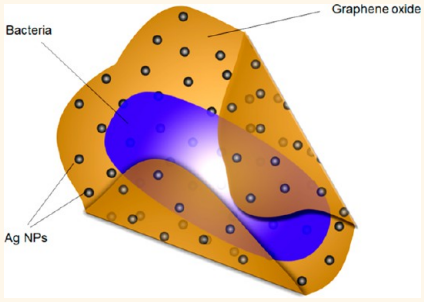

KEYWORDS: AgNPs · graphene oxide · Ag@dsDNA@GO composites · dsDNA · bacteria · tomato

Fresh market tomato is an important vegetable crop in the United States. It is grown on over 99 000 acres and was valued at $1.29 billion in 2012.[1] However, bacterial spot caused by *Xanthomonas perforans*, one of the major bacterial diseases affecting open field production worldwide, can lead to significant reduction in crop yield by 10−50% under conditions favorable to disease occurrence and spread. A recent estimate based on 2007−2008 production costs and market values showed that the monetary losses caused by bacterial spot in southwest Florida alone were $3090 per acre.[2] Disease management using different culture practices and disease-tolerant varieties has led to only mediocre results in tropical and subtropical regions, where the climatic conditions favor infection and spread of the disease. Chemical control using the antibiotic streptomycin was successfully used in the 1950s. However, in due course, strains resistant to streptomycin developed, making the antibiotic ineffective.[3] For many decades, the disease has also been managed using copper (Cu) bactericides, which have enhanced effectiveness when used in combination with ethylene-bis-dithiocarbamate (EBDC) fungicides (*e.g.*, maneb or mancozeb) based on the increased availability of free Cu^{2+} ions.[4,5] Unfortunately, widespread use of these bactericides has led to Cu resistance, and currently most of the strains isolated from Florida are resistant to copper.[6]

Disease management technologies, such as bacteriophages and systemic acquired resistance (SAR) inducers, have been under

* Address correspondence to tan@chem.ufl.edu.

Received for review July 8, 2013 and accepted September 9, 2013.

Published online September 09, 2013
10.1021/nn4034794

investigation for several years as alternatives to Cu bactericides.[7,8] Acibenzolar-S-methyl (ASM) is a SAR inducer that activates plant defense systems by increasing the transcription of stress-related genes. ASM has been shown to increase resistance of tomato to bacterial spot compared to untreated controls.[7] Bacteriophages have also shown promise as biological alternatives to conventional Cu bactericides. However, ensuring the efficacy of bacteriophages is challenging in field conditions due to limited phage viability and the specific environmental requirements for their multiplication. Thus, the tomato industry currently has very few effective materials for bacterial spot management.

In recent years, nanotechnology has been increasingly applied to the development of novel antimicrobials for the management of pathogenic bacteria affecting agricultural crops, humans, and animals. In particular, significant development in nanomaterials synthesis, such as polymeric, carbon-based, and metallic, has attracted researchers' attention toward applications in managing plant diseases caused by bacteria. Toxicity considerations, including negative environmental effects, have also led to the redesign of nanomaterials by tuning the size and shape and by surface modification, leading to increased antimicrobial activity and decreased ecological toxicity.[9] Most recently, an extensive study of the photocatalytic activity of TiO_2/Zn, TiO_2/Ag, and TiO_2 NPs on *X. perforans* has been carried out, indicating the potential of using nanoparticles in managing bacterial spot in tomato.[10]

To protect crops and animals from the effects of pathogens, polymeric and lipid-based edible film layers have been developed.[11] Several metal ions, such as Zn^{2+}, Cu^{2+}, and Ag^{+}, have been used to inactivate bacterial growth, although the mechanisms are not fully understood.[12] Because of the rather low antibacterial activity of metal ions, many researchers have focused on the use of nanomaterials to increase the effective antibacterial impact. This has led to the development of several types of nanomaterials, including the metallic nanoparticles Ag,[13] Cu,[14,15] CuO,[13,16] ZnO,[16] and TiO_2[10] with carbon-based nanomaterials, such as carbon nanotubes (CNTs),[16] as well as graphene oxide (GO)[14] and metallic nanoparticles formed on silica nanoparticles.[17]

Among the different types of nanoparticles, AgNPs have been used as effective biocides against a variety of pathogens,[18] fungi,[19] and viruses.[20,21] Researchers have debated the antibacterial activity of Ag^{+} ions and AgNPs and the mechanism underlying the bactericidal process. For example, one plausible theory holds that Ag^{+} ions interact with thiol, carboxyl, hydroxyl, amino, phosphate, and imidazole groups in proteins and enzymes on bacterial membranes, leading to serious structural deformation of the cell membrane. This is followed by the penetration of Ag^{+} ions into cells through the vulnerable membranes to inactivate

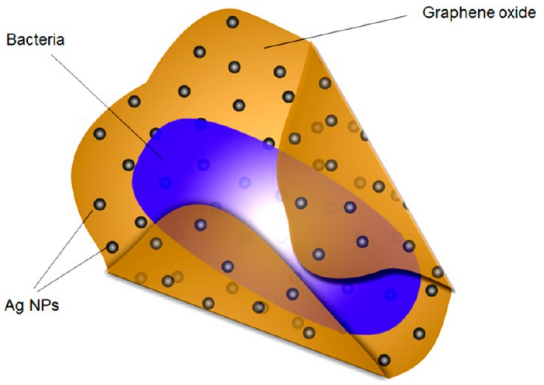

Scheme 1. Schematic illustration of interaction between Ag@dsDNA@GO composite and bacteria. When the bacterial cell adheres to the surface of GO, the GO wraps the cell *via* a swaddling process, so that AgNPs on the GO surface can interact with almost the entire cell surface.

enzymes, leading to suffocation, inhibition of cell replication, and eventual cell death. Several experiments have been performed on bacteria to evaluate the bactericidal effect of single AgNPs.[22] It is assumed that AgNPs interact with the bacterial membrane by way of Ag^{+} ions and that bacteria are killed by a combination of the bactericidal effects of AgNPs and released Ag^{+} ions, as noted above. To enhance the antibacterial activity of AgNPs and to increase the amount of released Ag^{+} ions, AgNPs have been prepared with different sizes,[23] shapes,[24] types of surface coatings,[25,26] and surface charges[27] for use in both aerobic and anaerobic environmental conditions.[28] However, the dependence of toxicity on these parameters is currently a major drawback in the use of bare AgNPs. In addition, agglomeration of bare AgNPs in contact with bacteria results in the loss of active surface area and weakening of antibacterial activity. To overcome these issues, graphene oxide, composed of a single layer of sp^2-bonded carbon atoms with active surface hydroxyl, epoxy, and carboxyl groups, can be used as a support material to grow AgNPs or to load presynthesized AgNPs. As a consequence of the synergistic effects of AgNPs and GO, these conjugates display extraordinary antibacterial activity compared to bare AgNPs.[29,30]

Thus, as an important practical application of nanotechnology, this paper reports a DNA-directed, facile, and one-step approach to synthesize Ag@dsDNA@GO composites[31] that display high antibacterial activity toward *X. perforans*, a model plant pathogenic bacterium, as shown schematically in Scheme 1. We further propose that the use of dsDNA as a template for growing AgNPs on GO enhances the synergistic effect between AgNPs and GO by controlling size, aggregation, and distribution of AgNPs and by increasing the adhesive force between Ag@GO composites and bacterial cell membranes.

RESULTS AND DISCUSSION

Synthesis and Characterization of Antibacterial Ag@dsDNA@GO. The morphology and size of AgNPs grown on dsDNA can be controlled according to the molar ratios of

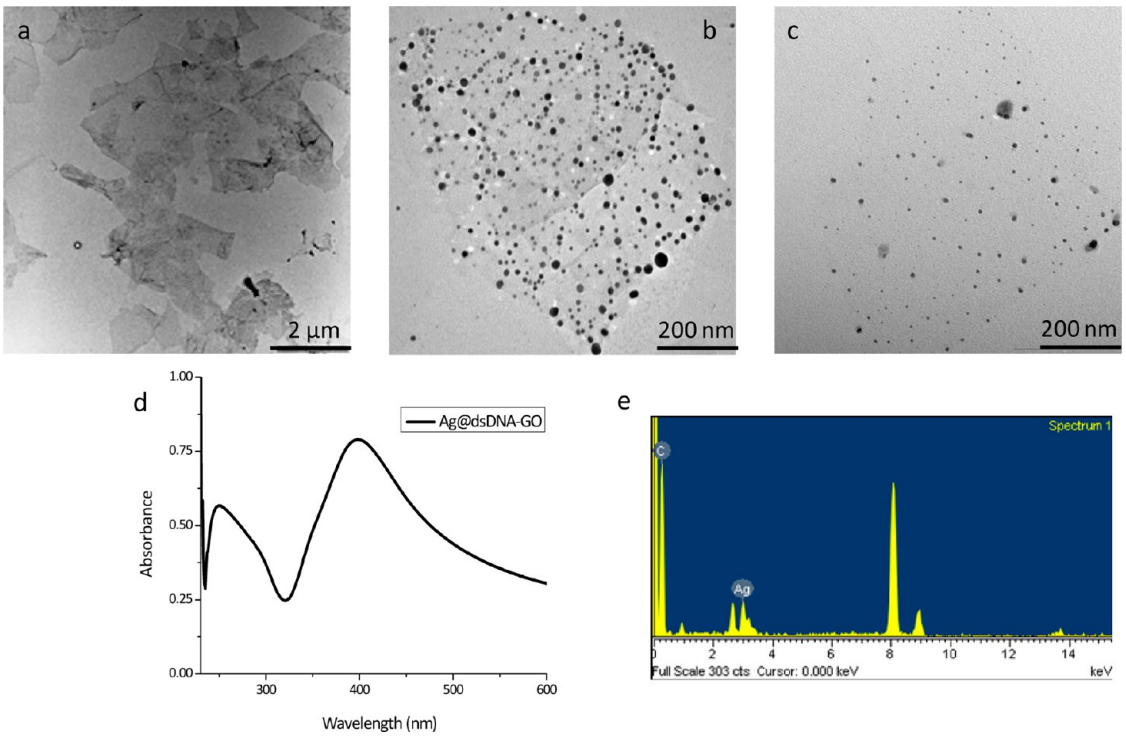

Figure 1. (a) TEM image of bare GO. (b) Ag@dsDNA@GO composite (Ag ~18 ± 3 nm). (c) Ag@dsDNA@GO composite (Ag ~5.0 ± 1.8 nm). (d) UV−vis absorption spectra of Ag@dsDNA@GO composite. (e) Dispersive X-ray spectroscopy (EDX) of Ag@dsDNA@GO composite.

dsDNA, reducing agent, and silver precursor. Silver(I) ions accumulate in the major groove of DNA at the phosphate and base moieties, thereby allowing control of the size and distribution of AgNPs on the GO surface, while also avoiding aggregation of nanoparticles. In addition, dsDNA acts as a stabilizer and increases the water solubility of GO and the Ag@GO composite.

The transmission electron microscopy (TEM) image of bare GO is shown in Figure 1a. The dsDNA-directed growth of AgNPs on the GO surface is clearly observed with TEM images (Figure 1b and c), which show Ag@GO composites with different sizes of AgNPs, 18 ± 3 and 5 ± 1.8 nm, respectively. The TEM images indicate that the two different sizes of dsDNA-directed AgNPs are monodispersed, and they uniformly cover the entire surface of GO without particle agglomeration. An increase in the concentration of reducing agent resulted in smaller sized AgNPs. For example, a molar ratio of silver precursor and reducing agent of 1:50 resulted in the formation of ~5 nm AgNPs. On the other hand, a decrease in concentration of reducing agent resulted in larger AgNPs. For example, a molar ratio of silver precursor and reducing agent of 1:5 resulted in ~18 nm AgNPs. We propose that the use of dsDNA as a template may provide three unique advantages: (1) synthesis of spherically shaped AgNPs on the GO surface, (2) minimization of aggregative growth to achieve uniform AgNP size, and (3) uniform distribution of AgNPs over the entire GO surface. The UV−vis spectrum of Ag@dsDNA@GO composites displays a broad absorption at ~395−400 nm (Figure 1d). EDX analysis shows the elemental composition of Ag@dsDNA@GO: silver and carbon (Figure 1e). The weight and atomic percentages of Ag in the Ag@GO composite given by EDX analysis are about 27% and 4%, respectively.

Antibacterial Activity of Ag@dsDNA@GO. Currently, no reports have conclusively documented the mechanism underlying the antibacterial activity of AgNPs and Ag@GO composites. However, according to the mechanism proposed by researchers, the GO sheet itself tends to nonspecifically attach and wrap bacteria, thereby increasing the interaction between the bacteria and GO.[32] Eventually, the AgNPs on GO cause direct and irreversible damage to the cell membrane by denaturing proteins located on the cell wall and then entering the cell through the bacterial cell-wrapping process. The AgNPs and Ag^+ ions released from AgNPs then react with thiol, carboxyl, hydroxyl, amino, phosphate, and imidazole groups existing on and in the cell for cell inactivation and death. Silver NPs, released Ag^+ ions, and silver-containing compounds have all been extensively used as universal germicides.[18] However, bare AgNPs exhibit much lower antibacterial activity than Ag@dsDNA@GO composites, possibly resulting from the agglomeration of bare AgNPs when in contact in medium with bacteria[25,33] and loss of active silver atoms in the presence of high bacterial counts.[25,33,34] In addition, modifying the AgNP surfaces with polymeric ligands to prevent agglomeration in living

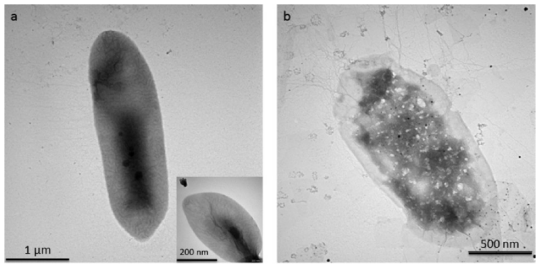

Figure 2. TEM images of *X. perforans* cells. (a) Before treatment (control) (inset: HRTEM image of *X. perforans*). (b) After treatment with 20 ppm Ag(18 nm)@dsDNA@GO composite for 20 h.

organisms has led to a decrease in the amount of released silver ions. In contrast, the highly enhanced superior antibacterial activity of our Ag@dsDNA@GO is attributed to the synergistic effect between GO and the AgNPs. In this case, we note that GO itself does interact with the cell membrane, but no antibacterial property toward *X. perforans* was observed in the plant pathogenic bacteria tested in our study. Strikingly, however, the Ag@dsDNA@GO composites did show excellent antibacterial efficacy compared to bare AgNPs and GO free in solution.

To test the antibacterial property of Ag@dsDNA@GO, a pathogenic strain of *X. perforans*, which causes bacterial spot on tomato, was used. The well-defined, intact membrane of rod-like *X. perforans* cells before treatment with 20 ppm Ag(18 nm)@dsDNA@GO composites and the newly divided normal *X. perforans* cell are shown with TEM images (Figure 2a and inset of Figure 2a). After 20 h incubation of *X. perforans* cells with 20 ppm Ag(18 nm)@dsDNA@GO composites, major morphological changes were observed, as shown in the TEM image (Figure 2b). The strong adhesion between Ag@dsDNA@GO composites and bacteria led to cell deformation and loss of the rod-shaped structure of the bacterium. The superior antibacterial properties of Ag@dsDNA@GO severely destroyed the cell membrane.

The changes in the rod shape of *X. perforans* were also observed with scanning electron microscopy (SEM) images before and after treatment with Ag@dsDNA@GO composites (Figure S1, Supporting Information). We propose that Ag@dsDNA@GO wraps around the *X. perforans* cell, leading to rapid cell deformation, in agreement with the synergism between GO and AgNPs, as noted above.[35]

The time-dependent antibacterial effect of the 20 ppm Ag@dsDNA@GO composite on *X. perforans* growth was studied with confocal microscopy (Figure 3). A mixture of SYTO 9 and propidium iodide (PI) at 1.67 and 18.3 mM, respectively, was used for LIVE/DEAD cell staining. The SYTO 9 dye stains bacterial cells with intact membranes fluorescent green, while the PI dye stains cells with damaged cell membranes fluorescent red. The zero-minute image (Figure 3a) shows *X. perforans* cells before treatment with 20 ppm Ag@dsDNA@GO composites. Most cells were alive, as indicated by the green fluorescence. After treatment of *X. perforans* cells with 20 ppm Ag@dsDNA@GO composites for 1 min, agglomeration of *X. perforans* cells was observed with initiation of *X. perforans* cell death indicated by red fluorescence (Figure 3b). This result confirms the highly enhanced antibacterial activity of Ag@dsDNA@GO composites within 1 min of treatment. Exposure of *X. perforans* to 20 ppm Ag@dsDNA@GO composites for 5, 10, 20, 40, and 60 min (Figure 3c through g) showed the same trend in *X. perforans* cell death.

In order to investigate the antibacterial properties of bare AgNPs, GO, Ag@GO, and Ag@dsDNA@GO on *X. perforans,* two different sizes of DNA-directed bare AgNPs (~18 and ~5 nm), Ag@dsDNA@GO composites with respective AgNPs of ~18 and ~5 nm and Ag@GO composite without DNA with ~8 nm AgNPs, were studied. Cell viability assay by direct plating of cells on yeast nutrient agar (YNA) media plates after exposure to the NPs showed that *X. perforans* is highly sensitive to bare AgNPs and Ag@GO and Ag@dsDNA@GO hybrid materials, but not to GO alone. The antibacterial activity toward *X. perforans* of ~18 nm bare AgNPs with different concentrations was studied (Figure 4a). The ~18 nm bare AgNPs did not display an effective antibacterial property up to 20 ppm concentration of AgNPs, but an incremental increase of *X. perforans* cell death was observed for 30−50 ppm concentrations. When AgNPs at a concentration of 50 ppm were used, ~45% *X. perforans* cell inactivation was observed, but an increase in antibacterial activity was observed for 100 and 200 ppm AgNPs, which killed ~99% of *X. perforans* cells. The antibacterial activity of GO and Ag@dsDNA@GO composites with respective AgNPs of ~18 and ~5 nm was determined by cell viability testing (Figure 4b). GO itself without AgNPs with respective concentrations of 20, 80, 100, and even 500 ppm caused no significant *X. perforans* cell death. However, in contrast to both bare AgNPs and GO alone, Ag@dsDNA@GO composites showed more efficacy in deactivating bacterial growth. Even at the lowest concentration, 20 ppm Ag(18 nm)@dsDNA@GO composites killed >95% of *X. perforans* cells. Furthermore, the synergistic effect between GO and Ag(18 nm), along with the capture effect provided by GO and dsDNA, significantly increased the antibacterial capability of Ag(18 nm)@dsDNA@GO composites. Interestingly, the Ag(5 nm)@dsDNA@GO composites displayed higher antibacterial activity than the Ag(18 nm)@dsDNA@GO composites. This can be attributed to the greater number of active Ag atoms, such that a concentration of 20 ppm of the Ag(5 nm)@dsDNA@GO conjugates was able to cause 100% of *X. perforans* cell death in 20 h. Furthermore, Ag(8 nm)@GO composites without DNA show much less antibacterial activity compared to Ag@dsDNA@GO composites. The use of 1 and 5 ppm Ag(8 nm)@GO composites does not display

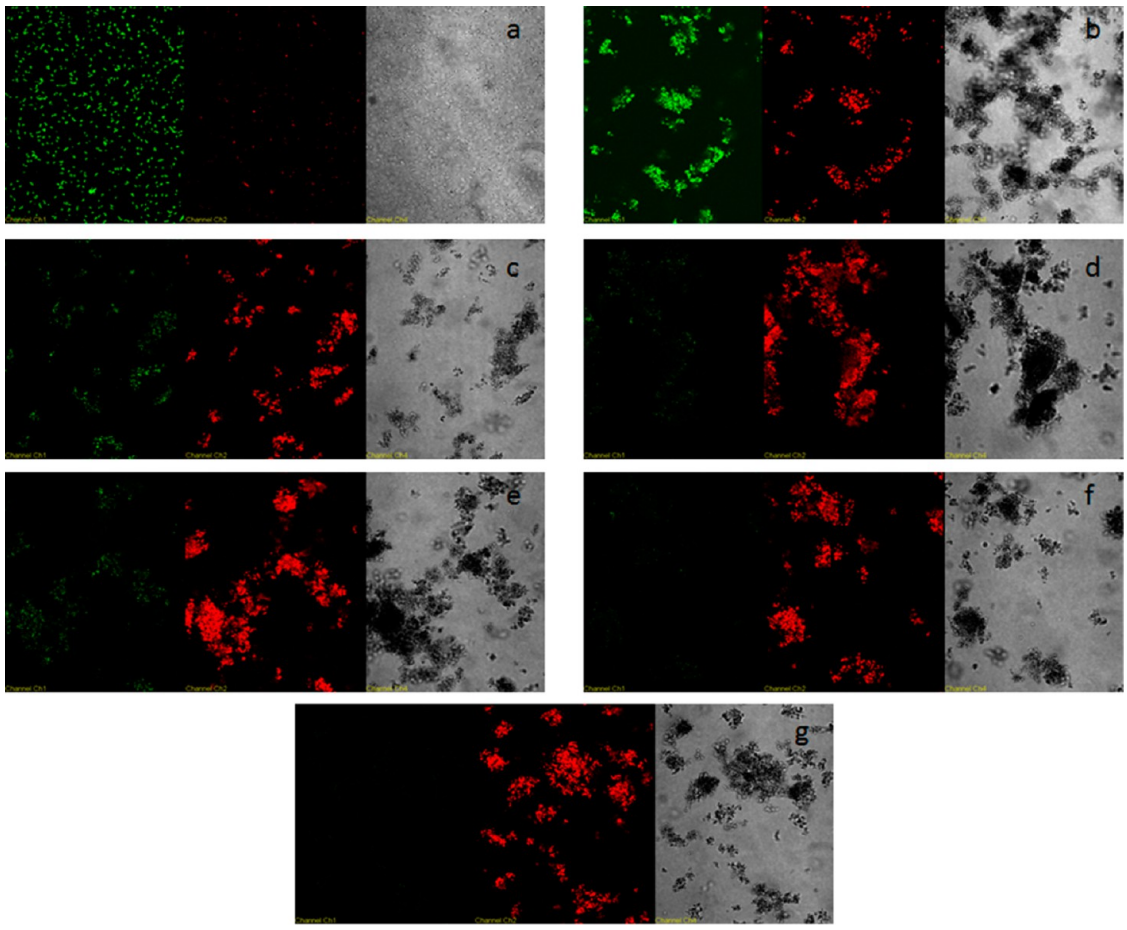

Figure 3. (a) Images of *X. perforans* cells. (b) Cells treated with 20 ppm Ag(18 nm)@dsDNA@GO for 1 min, (c) 5 min, (d) 10 min, (e) 20 min, (f) 40 min, and (g) 60 min, as monitored by confocal microscopy.

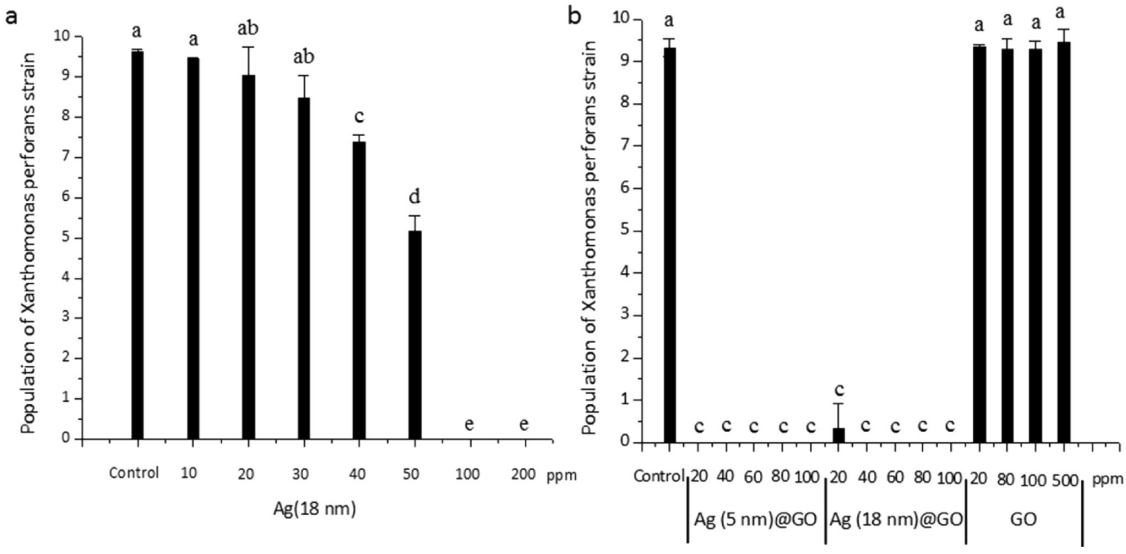

Figure 4. (a) Antibacterial activity of ~18 nm AgNPs grown on dsDNA with respective concentrations of 10, 20, 30, 40, 50, 100, and 200 ppm AgNP. (b) Antibacterial activity of Ag(5 nm)@dsDNA@GO and Ag(18 nm)@dsDNA@GO composites with concentrations of 0 (control), 20, 40, 60, 80, and 100 ppm Ag@dsDNA@GO conjugates and antibacterial activity of graphene oxide (GO) alone, with respective concentrations of 20, 80, 100, and 500 ppm. Column means labeled with different letters are statistically significantly different at $p \leq 0.005$ based on the Student–Newman–Keuls rest. The error bars represent the standard error of the mean.

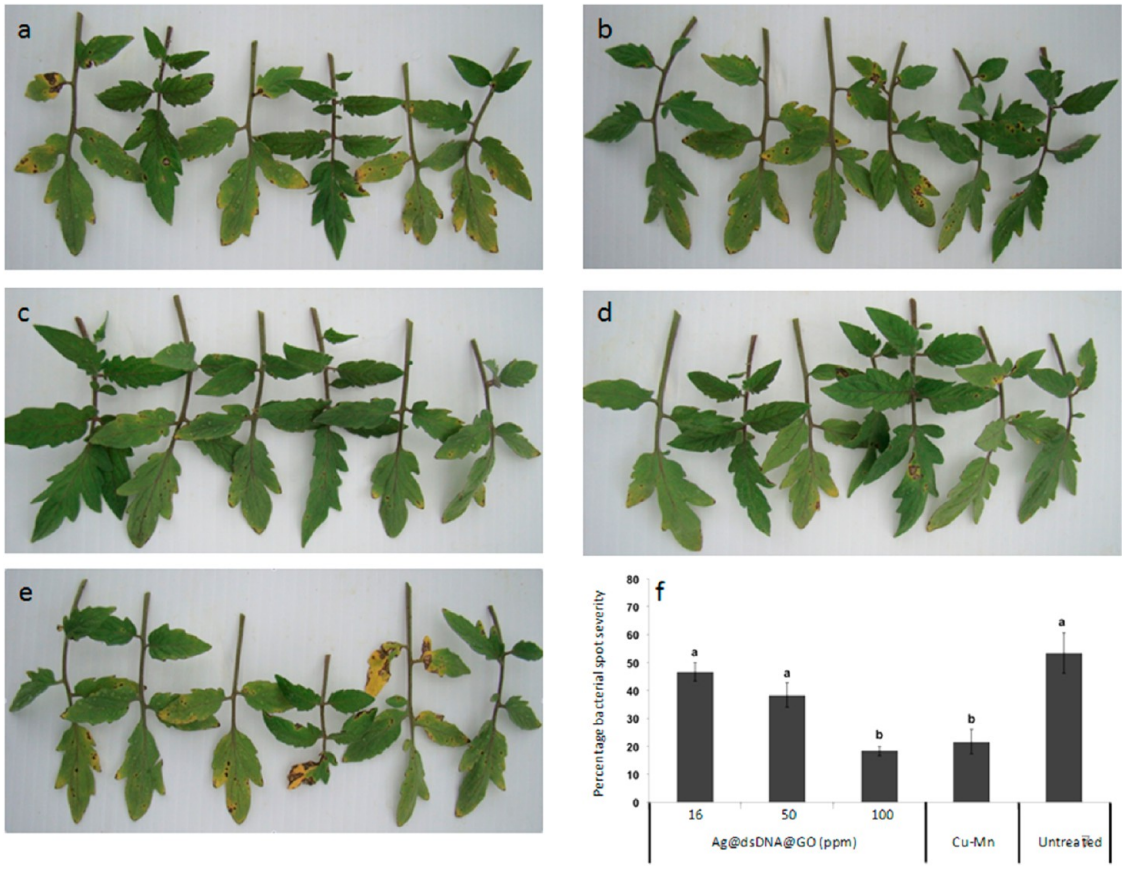

Figure 5. Treatment of tomato transplants with Ag(18 nm)@dsDNA@GO: (a) 16 ppm, (b) 50 ppm, (c) 100 ppm, (d) copper + mancozeb control, and (e) untreated control. (f) Three plants were tested for each treatment, and the trial was set up in a randomized complete block design. Cu−Mn represents copper (Kocide 3000; 2.1 g/L + mancozeb (Penncozeb 75DF; 1.2 g/L) treatment. Means followed by the same letter are not significantly different at $p \leq 0.05$ based on Student−Newman−Keuls test (LSD). The error bar represents standard error of the mean.

any effective antibacterial activity; however 20 ppm Ag(8 nm)@GO composites caused almost 50% of *X. perforans* cell death. The higher concentration of Ag(8 nm)@GO composites, 100 and 200 ppm, killed almost all bacterial cells with highly increased, significant antibacterial activity (Figure S2a, Supporting Information). In terms of antibacterial properties of Ag(8 nm)@GO and Ag(5 nm)-@dsDNA@GO in 20 ppm, we proved that Ag(5 nm)-@dsDNA@GO composites had a much higher antibacterial effect (at least 5-fold) compared to Ag(8 nm)@GO.

In addition, ~5 nm bare AgNPs with respective concentrations of 10, 20, 30, and 40 ppm only slightly inhibited *X. perforans* cell growth. However, use of 50 ppm ~5 nm AgNPs significantly increased antibacterial activity, with nearly 56% of *X. perforans* cells dead compared to 45% for ~18 nm bare AgNPs, due to the difference in size (and the number of particles present). Almost 99% of *X. perforans* cells were killed using 100 and 200 ppm ~5 nm AgNPs (Figure S3a, Supporting Information). These results also highlight a cornerstone of nanotechnology in general; that is, physicochemical properties are affected by size variation.

Moreover, Ag(5 nm)@dsDNA@GO composites were incubated with *X. perforans* cells at several low concentrations in order to determine the concentration dependence in terms of bacterial cytotoxicity (Figure S3b, Supporting Information). Concentrations of 1, 4, 8, and 12 ppm of Ag(5 nm)@dsDNA@GO composites were able to kill ~23%, ~44%, 52%, and 60% of *X. perforans* cells, respectively. The 16 ppm concentration of Ag(5 nm)@dsDNA@GO composites displayed the most promising antibacterial activity, with 100% *X. perforans* cell death.

Effectiveness of the Nanoparticles against Bacterial Spot on Tomato. Application of Ag@dsDNA@GO at 100 ppm on tomato transplants in the greenhouse experiment significantly reduced the severity of bacterial spot disease compared to the untreated control; the severity was on par with the current grower standard treatment, *i.e.*, copper + mancozeb (Figure 5). However, no significant reduction in bacterial spot severity was observed when plants were treated with 16 and 50 ppm Ag(18 nm)@dsDNA@GO, even though a numerical drop in bacterial spot severity was observed. This may have resulted from the limited adhesion of Ag@dsDNA@GO onto tomato leaves at these concentrations as a consequence of the numerous leaf hairs on the surface.

No phytotoxicity was observed on leaves from the application of Ag@dsDNA@GO. Therefore, this study points to the potential commercialization of this approach in the future management of bacterial diseases of vegetable crops worldwide. One of the key outcomes of the study is the effectiveness demonstrated by the Ag(18 nm)@dsDNA@GO composite at 100 ppm. The total amount of Ag present in this 100 ppm concentration of Ag@dsDNA@GO is at a very low amount, ~26.9 ppm. The extremely low amount of AgNPs in the material is very relevant, considering the possible regulatory consequence *vis-à-vis* EPA approval in the future commercialization of this technology. In Florida alone, about 200 000 pounds of elemental copper is applied annually on tomato (Steve Olson, personal communication). The development of DNA-directed nanoparticle formulation has the potential to significantly reduce the use of copper and transform agriculture in the U.S. by the development of cheap and eco-friendly products that may improve disease management, thereby saving millions of dollars in costs to the industry. Leaf and fruit samples of tomato plants treated with the effective nanoparticles will be analyzed at multiple time points after application using gas chromatography mass spectrometry after extraction of the samples using dispersive liquid−liquid microextraction, a method consistently used in pesticide residue analysis in tomatoes.[36,37] This will help us to study the uptake the Ag^+ on Ag nanoparticles into the leaves or the fruits. Furthermore, we realized that our current studies did not show any indication of any effect of nanoparticles on plant growth. However in further studies we will be analyzing plant growth patterns.

CONCLUSION

In summary, nanotechnology has been found to be highly useful in medical diagnostics, drug delivery, tissue engineering, *etc*. In this work, we have demonstrated that it also has a place in plant biology. The antibacterial activity of Ag@dsDNA@GO composites toward *X. perforans*, a model plant pathogenic bacterium, is enhanced by the synergistic effect between AgNPs and GO, as clearly shown by TEM, SEM, cell membrane staining, and cell viability assay. Optimal antibacterial activity was observed with 20 ppm Ag (18 nm)@dsDNA@GO and 16 ppm Ag (5 nm)@dsDNA@GO composites *in vitro* after an incubation of only 60 min. The Ag@dsDNA@GO displayed higher antibacterial behavior compared to the Ag@GO composite synthesized by different methods, bare AgNPs solution or bare GO solution. Finally, Ag@dsDNA@GO at 100 ppm was applied on tomato transplants in a greenhouse experiment, and significant reduction of disease caused by bacterial spot was visually observed compared to the untreated control and the control treated with copper + mancozeb. Application of Ag@dsDNA@GO did not induce any phytotoxic effect on plant leaves. Our preliminary results clearly show the great potential in using easily realized nanotechnology for existing severe problems in plants.

MATERIALS AND METHODS

Chemicals. Concentrated single-layer graphene oxide with 0.5−3 μm size range and 5g/L concentration was purchased from the Graphene Supermarket (Ronkonkoma, NY, USA) and used as received. Silver nitrate, ACS reagent, 99+% ($AgNO_3$), sodium borohydride ($NaBH_4$) 98%, and 4-(2-hydroxyethyl)-piperazine-1-ethanesulfonic acid (HEPES) were obtained from Sigma-Aldrich. Sodium nitrate ($NaNO_3$) was provided by Alfa-Aesar. Ultrapure water (18.2 M Ω; Millipore Co., Billerica, MA, USA) was used in the experiments.

Instrumentation and Characterization. One drop of Ag@dsDNA@GO composite dispersed in water was deposited on carbon-coated copper grids and allowed to dry overnight to obtain clear transmission electron microscopy images using a Hitachi H-7000 transmission electron microscope with a working voltage of 100 kV. For TEM images of bacterial cells before and after treatment with Ag@dsDNA@GO composite, one drop of 2% uranyl acetate (used as a negative stain in electron microscopy) was deposited on carbon-coated copper grids. After exposure to 2% uranyl acetate for 50 s, the excess uranyl acetate was removed with filter paper. Then, a bacterial cell suspension or suspension of bacterial cell−Ag@dsDNA@GO composite was deposited on the grid. A JEOL JEM-2010F field emission electron microscope coupled with spatially resolved energy dispersive X-ray spectroscopy (EDX) was also used for magnified images and further characterization of bacterial cell−Ag@dsDNA@GO composites. A field-emission scanning electron microscope (FESEM) (S-4000, Hitachi High Technologies America, Inc., Schaumburg, IL, USA) was used for FESEM images. Cultures were deposited onto poly-L-lysine-treated 0.2 μm Millipore filters, fixed with Trump's fixative (4% formalin, 1% glutaraldehyde), and stored overnight at 4 °C. Fixed cells were processed with the aid of a Pelco BioWave laboratory microwave (Ted Pella, Redding, CA, USA). Samples were washed in 1× phosphate-buffered saline (PBS), pH 7.24, postfixed with 1% buffered osmium tetroxide in 1× PBS, pH 7.24, water washed, dehydrated in a graded ethanol series (25%, 50%, 75%, 95%, 100%), and dried (TousimisAutosamdri-815, Tousimis Research Corporation, Rockville, MD, USA). Dried samples were mounted on carbon adhesive tabs on an aluminum specimen mount and Au/Pd sputter coated (DeskV, Denton Vacuum, Moorestown, NJ, USA). High-resolution digital micrographs were acquired with FESEM. An 1800 UV−vis spectrophotometer (Shimadzu Scientific Instruments, Columbia, MD, USA) was used for the absorption spectrum of Ag@dsDNA@GO composites and to determine the concentrations of DNA. An Olympus FV-500-IX81 confocal microscope (Olympus, Center Valley, PA, USA) having a 40× oil dispersion objective was used to monitor live and dead cells with a staining kit that includes a mixture of propidium iodide and green fluorescent nucleic acid stain (SYTO9).

Synthesis of DNA-Directed 18 nm Bare AgNPs in Solution and AgNPs on GO. The synthesis of DNA-directed AgNPs was accomplished through reduction of $AgNO_3$ with $NaBH_4$. DNA-1, 5′ AAT GTG CTC CCC CA GCGCGCTT FITC-3′, and DNA-2, 5′ TGG GGG AGC ACA TT-3′, were mixed together at the same concentration to obtain double-stranded DNA (dsDNA) *via* hybridization in HEPES buffer (pH 7.5) for 30 min. Then, $AgNO_3$ solution was added to a 1 μM dsDNA solution to make a final concentration

of 100 μM Ag^+ ions. The resulting mixture was incubated for 5 min, and freshly prepared $NaBH_4$ was injected dropwise into the mixture to give a final concentration of $NaBH_4$ of 500 μM. The final mixture was stirred for 30 min, washed twice with HEPES buffer, and centrifuged at 12 000 rpm for 15 min. The final products were redispersed in HEPES buffer for further characterization.

In order to grow AgNPs on GO, the graphene oxide solution was added to the dsDNA solution for adsorption of dsDNA on the GO. After 30 min incubation, the mixture was centrifuged, and excess dsDNA in the supernatant was decanted. The precipitated dsDNA−GO was redispersed in HEPES buffer, followed by addition of $AgNO_3$, which was prepared by the protocol mentioned above, to the dsDNA−GO mixture under vigorous stirring. After 10 min of incubation, freshly prepared $NaBH_4$ at a final concentration of 500 μM was injected dropwise into the mixture containing DNA, GO, and $AgNO_3$ for 30 min under vigorous stirring. Purification was achieved in the manner described above.

Synthesis of DNA-Directed 5 nm Bare AgNPs in Solution and on GO. In order to synthesize DNA-directed 5 nm bare AgNPs in solution and on GO, the protocol described above was followed, except the $NaBH_4$ was added dropwise into the mixture of dsDNA and $AgNO_3$ solution, or the mixture of dsDNA, $AgNO_3$, and GO, to give a final concentration of $NaBH_4$ of 5 mM. Purification was achieved in the manner described above. Finally, the sizes of DNA-directed bare AgNPs in solution and on the GO surface were measured by TEM and found to be about 5 $\pm$ 1.8 nm.

***In Vitro* Study.** The antibacterial activity of 5 nm bare AgNP and 5 nm AgNP grown on a dsDNA templated GO surface was studied (Figure S2). The bacterial cell killing property of 5 nm bare AgNP reached 56% *X. perforans* cell death at 50 ppm concentration (Figure S2a), but nearly 56% *X. perforans* cell death was achieved at almost 12 ppm of Ag(5 nm)@dsDNA@GO composites (Figure S2b).

Greenhouse Experiment. A greenhouse study was conducted on tomato transplants of the cultivar "FL47", at two-leaf stage, growing in soil-less potting medium (Sungro Metro-Mix 200 series; Sun Gro Horticulture Canada Ltd., Vancouver, BC, Canada) in expanded polystyrene trays of inverted pyramid design with cell size 4.4 $\times$ 4.4 $\times$ 6.3 cm. Plants were sprayed with the nanoparticles at 16, 50, and 100 ppm until runoff. Plants treated with copper (Kocide 3000) + mancozeb (Penncozeb 75DF) and untreated plants were kept as controls. Three plants were tested for each treatment, and the trial was set up in a randomized complete block design. Two hours after treatment, plants were inoculated with *X. perforans* race T4 strain GEV485 isolated from tomatoes in Wimauma, FL. Plants were bagged with a transparent plastic bag and kept for 48 h. The bags were opened, and the plants were kept at greenhouse conditions of 28−32 °C and 70% humidity for a period of 14 days. The percentage of bacterial spot severity was assessed at the end of the experiment based on a scale of 0−20 representing an increase of 5% in each scale with 0 representing no bacterial spot and 20 representing 100% bacterial spot severity. Leaves were also examined for phytotoxicity at the end of the experiment.

Conflict of Interest: The authors declare no competing financial interest.

Acknowledgment. I.O. acknowledges the Ministry of National Education, Republic of Turkey, for financial support for his doctoral studies. We thank Karen Kelley and Kim Backer-Kelley at the University of Florida Electron Microscopy and Bio-Imaging lab at the ICBR for assistance with observation of the samples. We appreciate the comments on the manuscript by Dr. Kathryn Williams as well as the suggestions of Dr. Jeff Jones. This work was supported by a grant from the National Science Foundation (NSF) and the University of Florida Opportunity Seed Grant 2010−2012. It was also supported by grants awarded by the National Institutes of Health (GM079359 and CA133086), the National Key Scientific Program of China (2011CB911000), NSFC (Grant 21221003), and China National Instrumentation Program 2011YQ03012412.

Supporting Information Available: The synthesis of DNA, Ag@dsDNA, and Ag@dsDNA@GO. Description of the method for the *in vitro* and greenhouse experiment. Chemicals and instruments used for SEM images. This material is available free of charge *via* the Internet at http://pubs.acs.org.

REFERENCES AND NOTES

1. NASS-USDA. *Vegetables 2011 summary*; **2012**; p 88.
2. VanSickle, J. J.; Weldon, R. The Economic Impact of Bacterial Leaf Spot on the Tomato Industry. *Proc. Fla. Tomato Inst.* **2009**, 31–32.
3. Thayer, P. L.; Stall, R. E. A Survey of Xanthomonas Vesicatoria Resistance to Streptomycin. *Proc. Fla. State Hort. Soc.* **1962**, *75*, 163–165.
4. Jones, J. B.; Jones, J. P. The Effect of Bactericides, Tank Mixing Time and Spray Schedule on Bacterial Leaf Spot of Tomato. *Proc. Fla. State Hort. Soc.* **1985**, *98*, 244–247.
5. Marco, G. M.; Stall, R. E. Control of Bacterial Spot of Pepper Initiated by Strains of Xanthomonas Campestris Pv. Vesicatoria That Differ in Sensitivity to Copper. *Plant Dis.* **1983**, *67*, 779–781.
6. Jones, J. B.; Woltz, S. S.; Jones, J. P.; Portier, K. L. Population Dynamics Xanthomonas Campestris Pv. Vesicatoria on Tomato Leaflets Treated with Copper Bactericides. *Phytopathology* **1991**, *81*, 714–719.
7. Obradovic, A.; Jones, J. B.; Momol, M. T.; Olson, S. M.; Jackson, L. E.; Balogh, B.; Guven, K.; Iriarte, F. B. Integration of Biological Control Agents and Systemic Acquired Resistance Inducers Against Bacterial Spot on Tomato. *Plant Dis.* **2005**, *89*, 712–716.
8. Huang, C.-H.; Vallad, G. E.; Zhang, S.; Wen, A.; Balogh, B.; Figueiredo, J. F. L.; Behlau, F.; Jones, J. B.; Momol, M. T.; Olson, S. M. Effect of Application Frequency and Reduced Rates of Acibenzolar-S-Methyl on the Field Efficacy of Induced Resistance Against Bacterial Spot on Tomato. *Plant Dis.* **2012**, *96*, 221–227.
9. Neal, A. What Can be Inferred from Bacterium-Nanoparticle Interactions about the Potential Consequences of Environmental Exposure to Nanoparticles? *Ecotoxicology* **2008**, *17*, 362–371.
10. Paret, L. M.; Vallad, E. G.; Averett, R. D.; Jones, B. J.; Olson, M. S. Photocatalysis: Effect of Light-Activated Nanoscale Formulations of TiO_2 on Xanthomonas Perforans, and Control of Bacterial Spot of Tomato. *Phytopathology* **2012**in press.
11. Cagri, A.; Ustunol, Z.; Ryser, E. T. Antimicrobial Edible Films and Coatings. *J. Food Prot.* **2004**, *67*, 83–848.
12. Kim, T. N.; Feng, Q. L.; Kim, J. O.; Wu, J.; Wang, H.; Chen, G. C.; Cui, F. Z. Antimicrobial Effects of Metal Ions (Ag^+, Cu^{2+}, Zn^{2+}) in Hydroxyapatite. *J. Mater. Sci. Mater. Med.* **1998**, *9*, 129–134.
13. Yoon, K.-Y.; Hoon Byeon, J.; Park, J.-H.; Hwang, J. Susceptibility Constants of Escherichia Coli and Bacillus Subtilis to Silver and Copper Nanoparticles. *Sci. Total Environ.* **2007**, *373*, 572–575.
14. Mallick, S.; Sharma, S.; Banerjee, M.; Ghosh, S. S.; Chattopadhyay, A.; Paul, A. Iodine-Stabilized Cu Nanoparticle Chitosan Composite for Antibacterial Applications. *ACS Appl. Mater. Interfaces* **2012**, *4*, 1313–1323.
15. Karlsson, H. L.; Cronholm, P.; Gustafsson, J.; Möller, L. Copper Oxide Nanoparticles are Highly Toxic: A Comparison between Metal Oxide Nanoparticles and Carbon Nanotubes. *Chem. Res. Toxicol.* **2008**, *21*, 1726–1732.
16. Hu, W.; Peng, C.; Luo, W.; Lv, M.; Li, X.; Li, D.; Huang, Q.; Fan, C. Graphene-Based Antibacterial Paper. *ACS Nano* **2010**, *4*, 4317–4323.
17. Kim, Y. H.; Lee, D. K.; Cha, H. G.; Kim, C. W.; Kang, Y. C.; Kang, Y. S. Preparation and Characterization of the Antibacterial Cu Nanoparticle Formed on the Surface of SiO_2 Nanoparticles. *J. Phys. Chem. B* **2006**, *110*, 24923–24928.
18. Sondi, I.; Salopek-Sondi, B. Silver Nanoparticles as Antimicrobial Agent: A Case Study on E. Coli as a Model for Gram-Negative Bacteria. *J. Colloid Interface Sci.* **2004**, *275*, 177–182.

19. Kim, K.-J.; Sung, W.; Suh, B.; Moon, S.-K.; Choi, J.-S.; Kim, J.; Lee, D. Antifungal Activity and Mode of Action of Silver Nano-Particles on Candida Albicans. *BioMetals* **2009**, *22*, 235–242.
20. Zodrow, K.; Brunet, L.; Mahendra, S.; Li, D.; Zhang, A.; Li, Q.; Alvarez, P. J. J. Polysulfone Ultrafiltration Membranes Impregnated with Silver Nanoparticles Show Improved Biofouling Resistance and Virus Removal. *Water Res.* **2009**, *43*, 715–723.
21. Elechiguerra, J.; Burt, J.; Morones, J.; Camacho-Bragado, A.; Gao, X.; Lara, H.; Yacaman, M. Interaction of Silver Nanoparticles with HIV-1. *J. Nanobiotechnol.* **2005**, *3*, 1–10.
22. Panáček, A.; Kvítek, L.; Prucek, R.; Kolář, M.; Večeřová, R.; Pizúrová, N.; Sharma, V. K.; Nevěčná, T. j.; Zbořil, R. Silver Colloid Nanoparticles: Synthesis, Characterization, and Their Antibacterial Activity. *J. Phys. Chem. B* **2006**, *110*, 16248–16253.
23. Dal Lago, V.; Franca de Oliveira, L.; de Almeida Goncalves, K.; Kobarg, J.; Borba Cardoso, M. Size-Selective Silver Nanoparticles: Future of Biomedical Devices with Enhanced Bactericidal Properties. *J. Mater. Chem.* **2011**, *21*, 12267–12273.
24. Pal, S.; Tak, Y. K.; Song, J. M. Does the Antibacterial Activity of Silver Nanoparticles Depend on the Shape of the Nanoparticle? A Study of the Gram-Negative Bacterium Escherichia Coli. *Appl. Environ. Microbiol.* **2007**, *73*, 1712–1720.
25. Kvitek, L.; Panaček, A.; Soukupova, J.; Kolar, M.; Večerova, R.; Prucek, R.; Holecova, M.; Zboril, R. Effect of Surfactants and Polymers on Stability and Antibacterial Activity of Silver Nanoparticles (NPS). *J. Phys. Chem. C* **2008**, *112*, 5825–5834.
26. Yang, X.; Gondikas, A. P.; Marinakos, S. M.; Auffan, M.; Liu, J.; Hsu-Kim, H.; Meyer, J. N. Mechanism of Silver Nanoparticle Toxicity Is Dependent on Dissolved Silver and Surface Coating in Caenorhabditis Elegans. *Environ. Sci. Technol.* **2011**, *46*, 1119–1127.
27. El Badawy, A. M.; Silva, R. G.; Morris, B.; Scheckel, K. G.; Suidan, M. T.; Tolaymat, T. M. Surface Charge-Dependent Toxicity of Silver Nanoparticles. *Environ. Sci. Technol.* **2010**, *45*, 283–287.
28. Xiu, Z.-m.; Zhang, Q.-b.; Puppala, H. L.; Colvin, V. L.; Alvarez, P. J. J. Negligible Particle-Specific Antibacterial Activity of Silver Nanoparticles. *Nano Lett.* **2012**, *12*, 4271–4275.
29. Xu, W.-P.; Zhang, L.-C.; Li, J.-P.; Lu, Y.; Li, H.-H.; Ma, Y.-N.; Wang, W.-D.; Yu, S.-H. Facile Synthesis of Silver@Graphene Oxide Nanocomposites and Their Enhanced Antibacterial Properties. *J. Mater. Chem.* **2011**, *21*, 4593–4597.
30. Das, M. R.; Sarma, R. K.; Saikia, R.; Kale, V. S.; Shelke, M. V.; Sengupta, P. Synthesis of Silver Nanoparticles in an Aqueous Suspension of Graphene Oxide Sheets and Its Antimicrobial Activity. *Colloids Surf. B* **2011**, *83*, 16–22.
31. Ocsoy, I.; Gulbakan, B.; Chen, T.; Zhu, G.; Chen, Z.; Sari, M. M.; Peng, L.; Xiong, X.; Fang, X.; Tan, W. DNA-Guided Metal-Nanoparticle Formation on Graphene Oxide Surface. *Adv. Mater.* **2013**, *25*, 2319–2325.
32. Liu, S.; Zeng, T. H.; Hofmann, M.; Burcombe, E.; Wei, J.; Jiang, R.; Kong, J.; Chen, Y. Antibacterial Activity of Graphite, Graphite Oxide, Graphene Oxide, and Reduced Graphene Oxide: Membrane and Oxidative Stress. *ACS Nano* **2011**, *5*, 6971–6980.
33. Shrivastava, S.; Bera, T.; Roy, A.; Singh, G.; Ramachandrarao, P.; Dash, D. Characterization of Enhanced Antibacterial Effects of Novel Silver Nanoparticles. *Nanotechnology* **2007**, *18*, 1–9.
34. Teeguarden, J. G.; Hinderliter, P. M.; Orr, G.; Thrall, B. D.; Pounds, J. G. Particokinetics *in Vitro*: Dosimetry Considerations or *in Vitro* Nanoparticle Toxicity Assessments. *Toxicol. Sci.* **2007**, *95*, 300–312.
35. Akhavan, O.; Ghaderi, E.; Esfandiar, A. Wrapping Bacteria by Graphene Nanosheets for Isolation from Environment, Reactivation by Sonication, and Inactivation by Near-Infrared Irradiation. *J. Phys. Chem. B* **2011**, *115*, 6279–6288.
36. Bidari, A.; Ganjali, M. R.; Norouzi, P.; Hosseini, M. R. M.; Assadi, Y. Sample Preparation Method for the Analysis of Some Organophosphorus Pesticides Residues in Tomato by Ultrasound-Assisted Solvent Extraction Followed by Dispersive Liquid–Liquid Microextraction. *Food Chem.* **2011**, *126*, 1840–1844.
37. Melo, A.; Cunha, S. C.; Mansilha, C.; Aguiar, A.; Pinho, O.; Ferreira, I. M. Monitoring Pesticide Residues in Greenhouse Tomato by Combining Acetonitrile-Based Extraction with Dispersive Liquid–Liquid Microextraction Followed by Gas-Chromatography–Mass Spectrometry. *Food Chem.* **2012**, *135*, 1071–1077.